

Aroyl hydrazone with large Stokes shift as a fluorescent probe for detection of Cu^{2+} in pure aqueous medium and *in vivo* studies

Romi Dwivedi^a, Saumya Singh^a, Brijesh Singh Chauhan^b, S. Srikrishna^b, Anoop Kumar Panday^c, Lokman H. Choudhury^c, Vinod Prasad Singh^{a,*}

^a Department of Chemistry, Institute of Science, Banaras Hindu University, Varanasi, 221005, India

^b Department of Bio Chemistry, Institute of Science, Banaras Hindu University, Varanasi, 221005, India

^c Department of Chemistry, Indian Institute of Technology Patna, Bihta, Patna, 801106, India

ARTICLE INFO

Keywords:

Fluorescent probe
Large Stokes shift
Static quenching
Bio imaging

ABSTRACT

An aroyl hydrazone based fluorescent probe, hpsh, has been developed for the selective detection of Cu^{2+} ions in pure aqueous medium by static fluorescence quenching. The fluorescence quenching of hpsh in the presence of Cu^{2+} takes place as a result of ground state complex formation through intramolecular charge transfer (ICT). Addition of Cu^{2+} ions changes the color of the solution from colorless to yellow-green which is clearly visible by naked eye. Large Stokes shift of hpsh prevents the self-quenching of the probe in absence of metal ions. The observed stoichiometry between Cu^{2+} and probe has been found as 1:2 (M: L). MTT assay of hpsh on fruit flies confirms that the probe is non-toxic and biocompatible. The plausible *in vivo* bioimaging application of the probe to detect Cu^{2+} in *Drosophila* gut tissues as well as in adult fruit fly has been investigated with excellent results.

1. Introduction

Significant possibilities in the field of fluorescent imaging tools capable of monitoring specific targets are continuously being explored in recent years [1,2]. In this regard, many attempts have been made to design small size molecular fluorophores with oriented chemical,

photophysical and biological properties that monitor toxic transition metal ions [3,4]. Cu^{2+} sensors have been the subject of intense study owing to its environmental significance, pivotal role in various physiological processes and in a number of neurodegenerative diseases [5–8]. Excess copper is considered as a biohazard as it is prone to produce reactive oxygen species (ROS), activating oxidative damage of protein, nucleic acid and lipids [9]. Although amount of copper can be calculated precisely by modern analytical techniques *viz.* Atomic absorption spectroscopy, Ion selective electrode and inductively coupled plasma mass spectroscopy [10,11], but these techniques bear some underlying drawbacks as these are relatively complicated, labor-intensive and costly. These techniques hamper the practical applications of the probe in biological field. Owing to high sensitivity, selectivity, easy detection by visual or instrumental methods and fast response, fluorescence is the most promising tool to meet the demand of in-field monitoring [12–14]. Therefore, the development of easily accessible and environment-friendly molecular probes for Cu^{2+} detection is still in

pursuit [15,16].

For bio application, a practical imaging agent must be stable, non-toxic, fairly soluble in water and produce complete quenching of fluorophore upon binding the analyte under study. However, in most of the cases self-quenching takes place in fluorophores showing small Stokes shifts *viz.* BODIPY, coumarin, rhodamine and fluorescein [17]. Though they are known to show strong fluorescence in dilute solutions but turn weakly fluorescent in concentrated solutions or in the solid state due to severe self-absorption among closely located molecules. Thus, a large Stokes shift is a great and significant property of a fluorophore [18]. Sie et al. (2017) [16] have reported a Schiff base sensor for the detection of Cu^{2+} , Co^{2+} and Hg^{2+} ions in water/DMSO matrix with real sample analysis, Aderinto et al. (2017) [19] have reported an ICT mechanism based Cu^{2+} sensor in tris-HCl buffer/DMF matrix with its application in real water samples, Bu et al. (2014) [20] have reported an indole base based Schiff base for the detection of Cu^{2+} in DMF, More and Shankarling (2017) [13] have reported a reversible and turn off fluorescence sensor for Cu^{2+} ion in ACN-HEPES buffer media. In all the above reported works there are some drawbacks *viz.* absence of biological application, mixed matrix solution, reversibility of the probe. Keeping these precedencies in view, in this paper, a highly selective quenching fluorescent probe with large Stokes shift for Cu^{2+} in aqueous media has been reported, which acts by way of static

* Corresponding author.

E-mail address: singvp@yahoo.co.in (V.P. Singh).

<https://doi.org/10.1016/j.jphotochem.2020.112501>

Received 24 June 2019; Received in revised form 12 March 2020; Accepted 14 March 2020

Available online 20 March 2020

1010-6030/ © 2020 Elsevier B.V. All rights reserved.

quenching mechanism. Herein, the current study attempts to gain a clear and deeper understanding of this phenomenon by means of *in vivo* trapping of Cu^{2+} in gut tissue of *Drosophila*.

2. Experimental

2.1. Reagents

Analytical reagent grade 2-hydroxypropiophenone (Sigma–Aldrich, USA), salicylic acid hydrazide (TCI Chemicals, India), solvents (Merck Chemicals, India), Chloride salts of Na^+ , K^+ , Mg^{2+} , Ca^{2+} , Ba^{2+} , Al^{3+} , Cr^{3+} , Mn^{2+} , Fe^{3+} , Co^{2+} , Ni^{2+} , Cu^{2+} , Zn^{2+} , Cd^{2+} , Hg^{2+} , Pb^{2+} (Merck Chemicals, India) were purchased and used without any further purification. Metal salt solutions were prepared in milli Q water.

2.2. Synthesis of probe

Synthesis of the probe hpsh was done by the reported method [21] by refluxing a mixture of salicylic acid hydrazide (10 mmol, 1.52 g) and 2-hydroxypropiophenone (10 mmol, 1.50 ml) solutions in dry ethanol in a round bottom flask for 3 h. After cooling the above solution to room temperature, a pale-yellow solid product was obtained. The product was filtered and washed thoroughly with ethanol. The compound was purified by recrystallization from hot ethanol and dried over anhydrous CaCl_2 in a desiccator.

2.3. Synthesis of hpsh- Cu^{2+} complex

Synthesis of hpsh- Cu^{2+} complex was done by reacting ethanolic solution of copper (II) chloride (5 mmol) with hpsh solution (10 mmol) in 1:2 (M: L) molar ratio in a round bottom flask. The reaction mixture was stirred on a magnetic stirrer at room temperature for half an hour to precipitate a green colored product. The product was filtered in a glass crucible, washed several times with ethanol and finally with diethyl ether, and dried in a desiccator at room temperature (Scheme 1).

2.4. UV-vis and fluorescence measurements

For UV-vis titration and fluorescence titration experiments, 50 μM and 5 μM aqueous solution of hpsh were used at room temperature. Milli Q water was used to prepare solution of the cations. Host-guest binding ratio was obtained from Job's plot. The binding constant (K_b) has been obtained from the fluorescence quenching data using modified Benesi-Hildebrand equation (Eq. 1) [22].

$$\log (F^0 - F)/F = \log K_b + n \log [Q] \quad (1)$$

i.e. $\log [(F^0 - F)/F]$ vs function of $\log [Q]$, a straight line appears in the plot, whose slope corresponds to n (binding number), K_b is the binding constant, F^0 is the initial emission intensity of hpsh when there was no metal ion, F is the emission intensity of hpsh after addition of metal ion and $[Q]$ is the concentration of Cu^{2+} .

The limit of detection of the receptor hpsh for Cu^{2+} was calculated from the plot of fluorescence emission intensity vs concentration of

added Cu^{2+} . To find out standard deviation (σ), the emission intensity of hpsh without Cu^{2+} was measured 10 times. The limit of detection (LOD) was then calculated from the definition given by IUPAC and the slope of the Stern-Volmer plot according to the equation (Eq. 2) [23]:

$$\text{LOD} = 3\sigma/K \quad (2)$$

Where, σ is the standard deviation of 10 independent blank measurements and K is the slope of Stern-Volmer plot (Eq. 3) *i.e.* F^0/F versus $[\text{Cu}^{2+}]$.

$$F^0/F = 1 + K_{\text{SV}}[Q] = 1 + k_q\tau^0 [Q] \quad (3)$$

K_{SV} is the Stern–Volmer quenching constant, τ^0 is average fluorescence lifetime of fluorophore *i.e.* 10^{-8} s; k_q *i.e.* K_{SV}/τ^0 , is quenching rate constant [24,25].

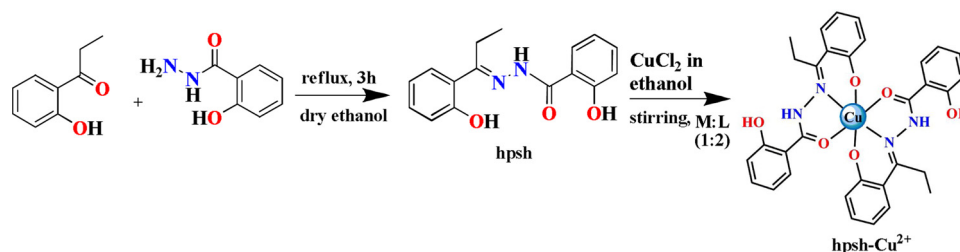
2.5. Median lethal dose (LD_{50}) determination

In toxicology, to examine the median lethal dose of hpsh, age matched virgin female and male oregonR⁺ flies were collected. The 10 virgin females were genetically crossed with 10 male flies in separate vials having different hpsh concentrations of 10 μM , 50 μM , 100 μM , 250 μM , 500 μM , 1000 μM and 2000 μM . The flies were grown in untreated food considered as control. After 15 days of treatment, their F1 adult progeny were scored in reference to control to assess lethality of hpsh. All experiments were performed in triplicate.

2.6. Fly culture

The wild type Oregon-R⁺ fruit flies obtained from Bloomington *Drosophila* stock center, Indiana, USA, were cultured on standard corn meal agar media at 24 ± 1 °C in BOD incubator. The wild type Oregon R⁺ adult *Drosophila* (fruit fly) and the gut tissues of *Drosophila* third instar larvae were used for the bioimaging studies. The untreated flies considered as control. Flies were incubated with 10 μM hpsh, 10 μM Cu^{2+} alone and 10 μM hpsh + 10 μM Cu^{2+} respectively in separate food vials. All experiments were performed in triplicate. Their F1 progenies had grown to adult. The 15 days old flies were selected for bioimaging studies through fluorescence microscopy.

The gut tissues were dissected in PBS (pH 7.4) with the aid of fresh fine needles under the Stereomicroscope (Magnus Zoom Star-V). The dissected tissues were incubated separately with 10 μM hpsh and 10 μM Cu^{2+} in Maximo cavity slides for 60 min. at room temperature. Simultaneously, gut tissues were incubated with hpsh for 40 min. and were subsequently incubated with Cu^{2+} for 20 min. in a separate cavity slide. The untreated gut tissues were considered as control. Tissues were washed twice with PBS after each consecutive step of treatment. The processed tissues were mounted with PBS on plane glass slide and observed under the Nikon NiU-Upright fluorescence microscope to evaluate the intracellular fluorescence intensity.



Scheme 1. Synthesis of hpsh and hpsh- Cu^{2+} complex.

3. Results and discussion

3.1. Spectroscopic characterization of *hpsh* and *hpsh-Cu²⁺*

3.1.1. *hpsh*

Yield (77 %). M.P. 239 °C. Anal. Calc. for $C_{16}H_{16}N_2O_3$ (284.31): C, 67.50; H, 5.56; N, 9.76. Found: C, 67.35; H, 5.46; N, 9.87 %. HR-MS: $[M + Na]^+$, m/z , 307.10. IR (cm^{-1} , KBr): $\nu(O-H)$ 3415, $\nu(N-H)$ 3326, $\nu(C=O)$ 1644, $\nu(C=N)$ 1614, $\nu(N-N)$ 926. ^{1}H NMR data: 1.23 (3H, $J = 7.2$ Hz, CH_3); 2.90 (2H, CH_2), 6.903–8.005 (Ar-H), 11.68 (s, 1H, NH), 13.19 (s, 1H, OH). ^{13}C NMR (DMSO- d_6): 11.05 (CH_3); 21.22 (CH_2); 113.47–132.84 (aromatic carbons); 83.163.01 (C=N); 166.76 (C-OH); 185.27 (C = O).

3.1.2. *hpsh-Cu²⁺*

Green, Yield (73 %). M.P. 260 °C. Anal. Calc. for $C_{32}H_{30}CuN_4O_6$ (630.15): C, 60.89; H, 4.79; N, 8.75; Cu, 10.04. Found: C, 60.69; H, 4.78; N, 8.78; Cu, 10.01 %. HR-MS: $[M + H]^+$, m/z , 631.16. IR (cm^{-1} , KBr): $\nu(OH-)$, 3380; $\nu(N-H)$ 3323; $\nu(C=O)$, 1622; $\nu(CN)$, 1597; $\nu(CO=)$, 1361; $\nu(NN-)$, 957; $\nu(Cu-O)$, 536; $\nu(Cu-N)$, 436.

In the IR spectra of *hpsh* (Fig. S1), the bands for $-CN$ and $>CO=$ groups observed at 1614 cm^{-1} and 1644 cm^{-1} , respectively, are shifted to lower frequency ($17\text{--}22\text{ cm}^{-1}$) in its Cu^{2+} complex (Fig. S2) suggesting coordination of the nitrogen atom of $>CN$ and oxygen atom of $>CO=$ groups with metal. The band corresponding to amine ($>N-H$) group observed at 3326 cm^{-1} in *hpsh* shows a negligible shift in *hpsh-Cu²⁺* complex indicating non-involvement of $>N-H$ group in bonding [26]. The presence of a new $(C-O^-)$ band in *hpsh-Cu²⁺* complex at 1361 cm^{-1} , suggests bonding of *hpsh* to Cu^{2+} via phenolate-O [27]. The $\nu(NN-)$ band in *hpsh* is shifted to higher wave number (31 cm^{-1}) in the complex suggesting the involvement of one of the nitrogen atoms of $>NN<-$ group in bonding [28]. The bands at 3415 cm^{-1} in *hpsh* and 3380 cm^{-1} in Cu^{2+} complex, are assigned to phenolic-OH [29].

The 1H NMR signals for $-COH$ and $>NH-$ protons in *hpsh* (Fig. S3 ESI) appear at 13.632 and 11.158 ppm, respectively [21]. The signals observed at 8.05–6.89, 2.49 and 1.23 ppm are assigned for aromatic, CH_2 and CH_3 protons, respectively. ^{13}C NMR (Fig. S4 ESI) spectrum of *hpsh* exhibits signals at 158.96, 156.27, 133.64, 131.18–116.86, 19.39 and 10.25 ppm for $(C=O)$, (COH) , $(CN=)$, aromatic, CH_2 , and CH_3 carbons, respectively. The molecular ion peak observed at $m/z = 307.10$ in HR-MS spectrum of *hpsh* (Fig. S5, ESI) correspond well to $[M + Na]^+$ validating the molecular formula $C_{16}H_{16}N_2O_3$. The HR-MS spectrum of the *hpsh-Cu²⁺* complex shows a molecular ion peak at m/z , 631.16 $[M + Na]^+$ confirms the molecular formula, $C_{32}H_{30}CuN_4O_6$ (Fig. S6, ESI).

3.2. Absorption studies

The strong peak observed at 340 nm in the absorption spectrum of *hpsh* was mainly due to n to π^* transitions of imine group. Another strong peak present in the high-energy region of 294 nm was due to π to π^* transition of aromatic group of *hpsh* (Fig. 1a) [30]. The absorption spectra of *hpsh* was investigated by the presence of several mono/bi/trivalent metal salts viz. Na^+ , K^+ , Ba^{2+} , Ca^{2+} , Al^{3+} , Cr^{3+} , Mn^{2+} , Fe^{3+} , Co^{2+} , Ni^{2+} , Zn^{2+} and Hg^{2+} in 50 μM aqueous solution of *hpsh* showed no significant change (Fig. 1b) while a distinct change was observed upon the addition of Cu^{2+} ions. In the presence of Cu^{2+} , the absorption spectra of *hpsh* showed a major band at 374 nm with a red-shift (34 nm) and 298 nm.

UV-vis titration (Fig. 2) was performed to study the binding behavior of *hpsh*. The successive addition of Cu^{2+} up to 0.7 eq. resulted an increase in absorbance while further addition of Cu^{2+} up to 1 equivalent caused a decrease in absorbance at $\lambda_{max} = 374\text{ nm}$ indicating complex formation by $C=N$ coordination in ground state in 1:2 (M: L) stoichiometric ratio [19].

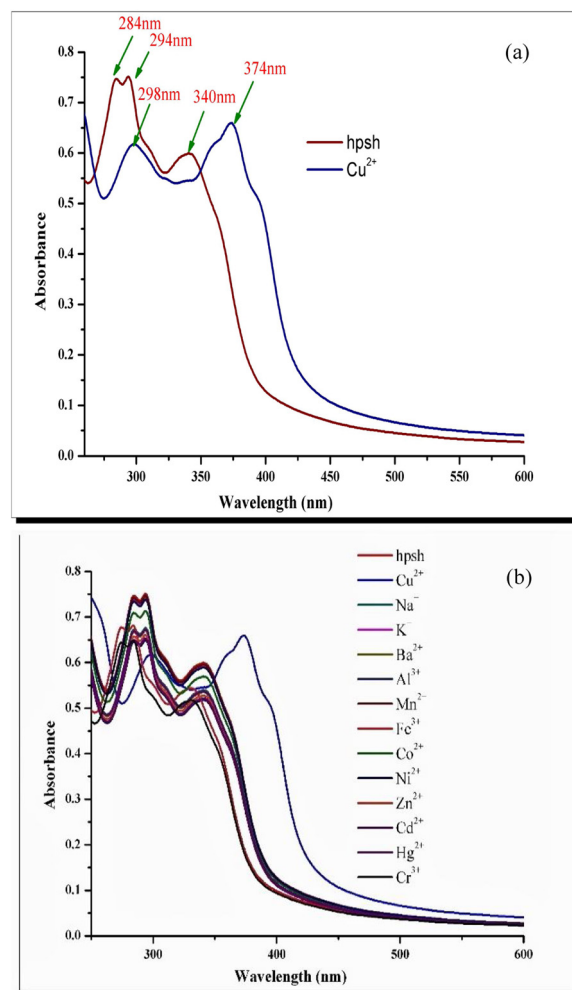


Fig. 1. UV-vis spectra of 50 μM aqueous solution of *hpsh* (a) upon addition of 1 equivalent of aqueous Cu^{2+} ions. (b) Upon addition of 1 equivalent of aqueous Na^+ , K^+ , Ba^{2+} , Al^{3+} , Cr^{3+} , Mn^{2+} , Fe^{3+} , Co^{2+} , Ni^{2+} , Zn^{2+} , Cd^{2+} , Hg^{2+} and Cu^{2+} ions.

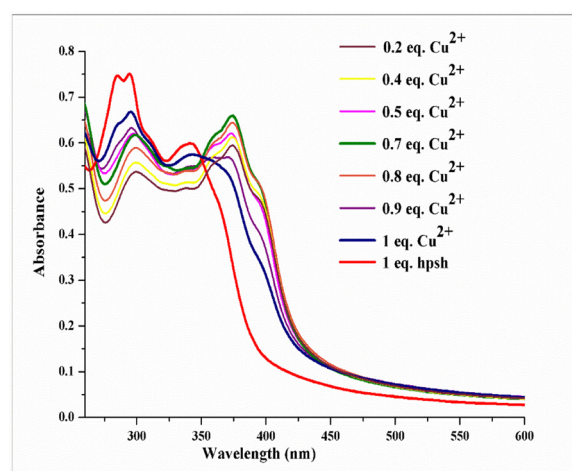


Fig. 2. UV-vis titration spectra of 50 μM aqueous solution of *hpsh* showing increased absorbance up to 0.7 eq. of aqueous Cu^{2+} ion while further addition up to 1 equivalent resulted in decreased absorbance.

To quantify the reaction ratio between *hpsh* and Cu^{2+} ions, a Job's plot from UV-vis spectra was constructed by changing the concentration of Cu^{2+} ions, which clearly indicated 1:2 (M: L) stoichiometry

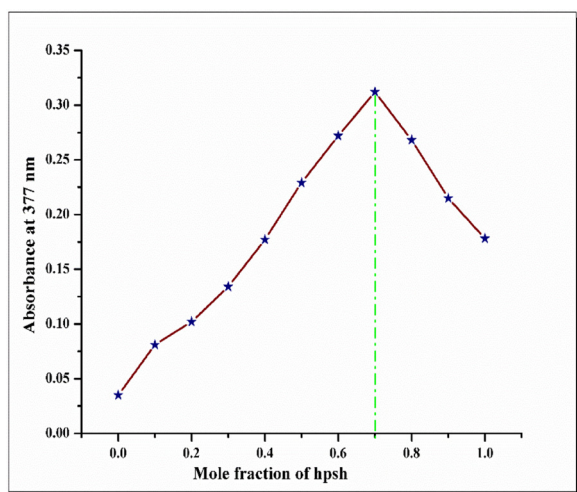


Fig. 3. Job's plot for hpsh-Cu²⁺ complex showing 1:2 (M: L) stoichiometry.

(Fig. 3) for hpsh-Cu²⁺ complex.

3.3. Emission studies

The fluorescence emission spectra of pure hpsh showed strong fluorescence at 517 nm (λ_{ex} : 298 nm) with 219 nm Stokes shift. The peak at 590 nm is due to Rayleigh scattering. Emission intensity of hpsh was examined against aforementioned ions. As shown in Fig. 4a,

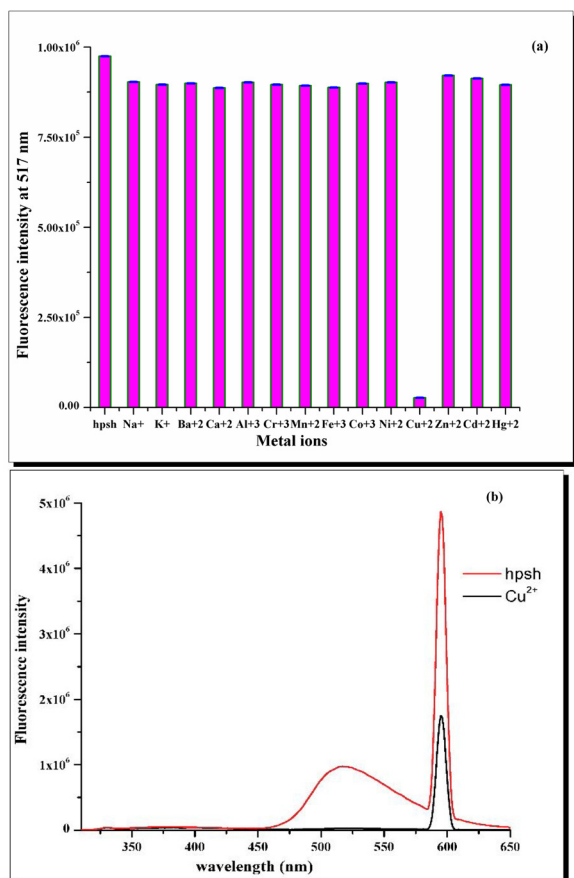


Fig. 4. (a) Fluorescence bar diagram of aqueous solution of hpsh (5 μM) + Mⁿ⁺ (10 μM); Mⁿ⁺ = Na⁺, K⁺, Ba²⁺, Ca²⁺, Al³⁺, Cr³⁺, Mn²⁺, Fe³⁺, Co²⁺, Ni²⁺, Zn²⁺, Cd²⁺ and Hg²⁺. (b) Fluorescence spectra of hpsh on addition of 2 equivalents of aqueous Cu²⁺ ions at λ_{em} : 517 nm (λ_{ex} : 298 nm).

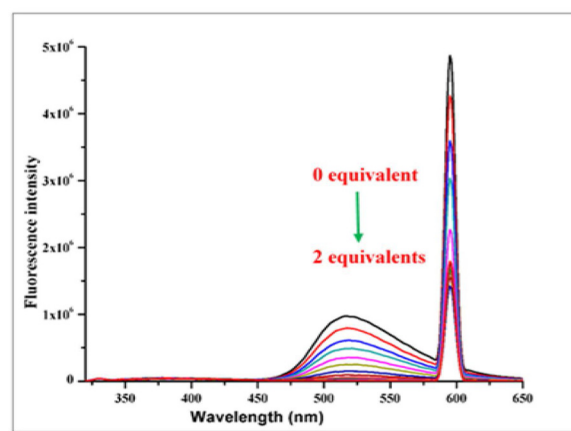


Fig. 5. Fluorescence titration of 5 μM aqueous solution of hpsh at λ_{em} : 517 nm (λ_{ex} : 298 nm) upon addition of 0-2 equivalents (10 μM) Cu²⁺ ion.

fluorescence spectra of hpsh was not noticeably affected by cations under test except Cu²⁺. On adding 2 equivalents aqueous Cu²⁺ ions to 5 μM aqueous solution of hpsh, there was drastic decrease in fluorescent intensity resulted in complete quenching of fluorescence of hpsh (Fig. 4 b). Fluorescence turn-off of hpsh by Cu²⁺ was further explained by emission titration of 5 μM aqueous solution of hpsh (Fig. 5).

Upon addition of successive amount of Cu²⁺ up to 1 equivalent, the intensity of the maximum emission at 517 nm quenched completely. Further addition of Cu²⁺ up to 2 equivalents reflected no change in the emission intensity of hpsh. To evaluate the selectivity of hpsh towards Cu²⁺, an interference experiment between Cu²⁺ and rest of the metals with hpsh was performed. It was observed from Fig. 6 that no interference was there for the detection of Cu²⁺ in the presence of Na⁺, K⁺, Ba²⁺, Ca²⁺, Al³⁺, Cr³⁺, Mn²⁺, Fe³⁺, Co²⁺, Ni²⁺, Zn²⁺, Cd²⁺ and Hg²⁺.

3.4. pH effect

The influence of pH on the probe has been studied by recording the absorption spectra of hpsh in the acidic, basic and neutral solution. The UV-vis. spectrum of hpsh at acidic pH showed slight shift in wavelength with a decrease in absorbance compared to neutral pH, while at basic pH, a new peak generated at higher wavelength due to deprotonation of hpsh followed by extension in conjugation. (Fig. S7) Like absorption spectra, the influence of pH on the probe hpsh has also been explained

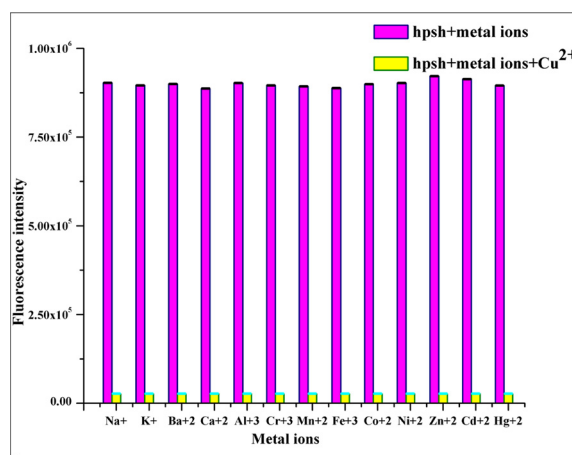


Fig. 6. Interference of other metal ions in binary mixture solution of aqueous hpsh (5 μM) + Cu²⁺ (5 μM) + Mⁿ⁺ (10 μM) at λ_{em} : 517 nm (λ_{ex} : 298 nm); Mⁿ⁺ = Na⁺, K⁺, Ba²⁺, Ca²⁺, Al³⁺, Cr³⁺, Mn²⁺, Fe³⁺, Co²⁺, Ni²⁺, Zn²⁺, Cd²⁺ and Hg²⁺.

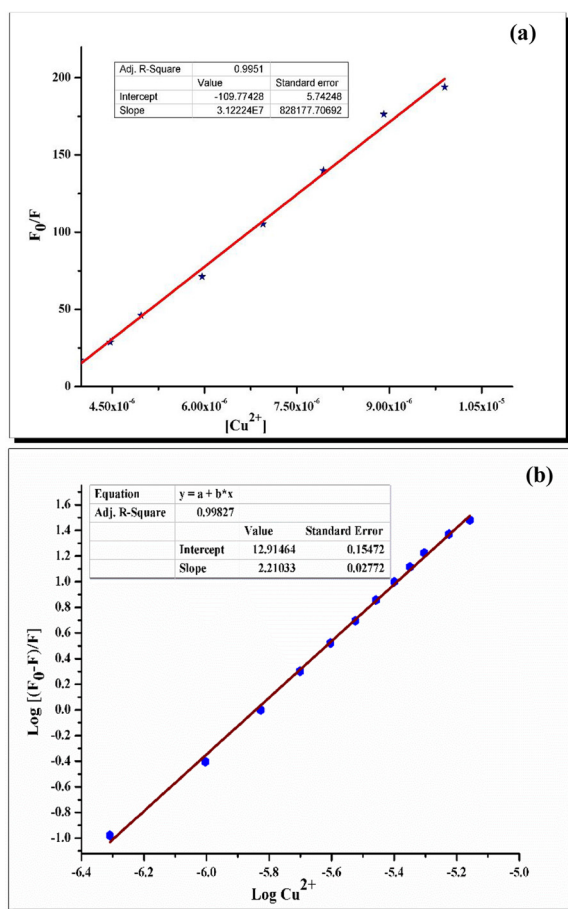


Fig. 7. a) Emission intensities of hpsh (5 μM) vs. $[\text{Cu}^{2+}]$ at λ_{em} :517 nm (λ_{ex} : 298 nm) (b) Benesi–Hildebrand plot for hpsh with Cu^{2+} for 1:2 (M: L) complexation.

by fluorescence study (Fig. S8). At λ_{ex} : 298 nm, the emission spectra of hpsh in acidic and neutral medium followed similar pattern while in basic medium hpsh showed no emission. Since at this excitation wavelength there was no absorbance in the UV–vis spectrum.

3.5. Detection limit and binding constant

The detection limit (LOD) of hpsh (5 μM) at λ_{em} = 517 nm (λ_{ex} = 298 nm) was calculated according to the definition of IUPAC [31] and the value from the linear fitting of Stern–Volmer plot [23] is 3.03×10^{-7} M in the linearity range of 4.0×10^{-6} – 1.05×10^{-5} M (R^2 = 0.9951) (Fig. 7(a)). It is under the regulatory limits given by WHO and USEPA [32,33]. Furthermore, the binding constant for hpsh- Cu^{2+} complex was calculated to be 8.21×10^{12} M^{-1} by the linear fitting of the fluorescence titration plot in modified Benesi–Hildebrand

expression [22]. From Fig. 7(b), very good linear relationship was observed ($R \approx 0.998$), and the value of n is close to 2. This means that binding ratio of hpsh- Cu^{2+} is in the ratio of 1:2 (M: L). This information was also supported by UV–vis Job's plot analysis.

3.6. Binding mode of hpsh- Cu^{2+} complex and Mechanism of quenching

It is clear from the earlier discussion about the structural characterization of hpsh- Cu^{2+} complex by FT-IR spectra and HR-MS data that Cu^{2+} coordinates with nitrogen atom of $>\text{CN}$, oxygen atom of $>\text{CO}=\text{O}$ and phenolate-O of the probe hpsh.

Intramolecular charge transfer takes place in system when there is direct attachment of the receptor to the electron donating/withdrawing groups in conjugation to fluorophore [34,35]. The hpsh is formulated such in a way as all the functional groups present in probe come in the proximity of the fluorophore moiety of the probe. Fig. 8(a). When the system is irradiated, the fluorophore undergoes intramolecular charge transfer between donor and acceptor. The donors are the $-\text{OH}$ groups in hpsh and the receptor is the Cu^{2+} chelating moiety. An effective fluorescence quenching process happens when receptor Cu^{2+} chelating moiety incorporates into fluorescence motifs and an apparent red shift is observed in the absorption spectrum due to the ICT becoming more developed. The chelation between hpsh and Cu^{2+} is facilitated by the coordination from: (i) the imine group, $\text{C}=\text{N}$ (ii) the carbonyl group and (iii) the phenolate oxygen group (Fig. 8(b)).

UV–vis spectral changes of hpsh before and after the addition of Cu^{2+} suggested the quenching mechanism to be static in nature due to the complex formation in the ground state. (Fig. S9). Stern–Volmer quenching constant calculated from the equation (Eqn. 3) was also employed to differentiate static quenching from dynamic quenching. For dynamic quenching k_q i.e. K_{SV}/τ^0 (quenching rate constant) of various quenchers is limited to 2.0×10^{10} $\text{L mol}^{-1} \text{s}^{-1}$ [36,37]. While in our case, calculated k_q (K_{SV}/τ^0) is 3.12×10^{15} $\text{L mol}^{-1} \text{s}^{-1}$, that is 50,000 times larger than 2.0×10^{10} $\text{L mol}^{-1} \text{s}^{-1}$ supporting static nature of the quenching, K_{SV} is obtained from the detection limit plot of hpsh- Cu^{2+} complex i.e. 3.12×10^7 L mol^{-1} (Fig. 7(a)).

3.7. Significance of large Stokes shift

Self-quenching takes place mainly in fluorophores having small Stokes shift. Thus, large Stokes shift is an important property of fluorophore to prevent self-quenching in solid state (Fig. S10) [17]. The Stokes shift ($\nu_A - \nu_F$) explains the difference in the properties and structure of the fluorophore between the ground state (S^0) and the first excited state (S_1) according to the equation (Eq. 4) [38].

$$(\nu_A - \nu_F) = (1/\lambda_A - 1/\lambda_F) \times 10^7 \text{ cm}^{-1} \quad (4)$$

Intramolecular charge-transfer between HOMO and LUMO of the chromophore, inter and intra molecular hydrogen bonding of hpsh with water due to the presence of the polar groups are the responsible causes for the observed Stokes shift. Polar solvents yield larger Stokes shift values than non-polar solvents owing to their more favored hydrogen

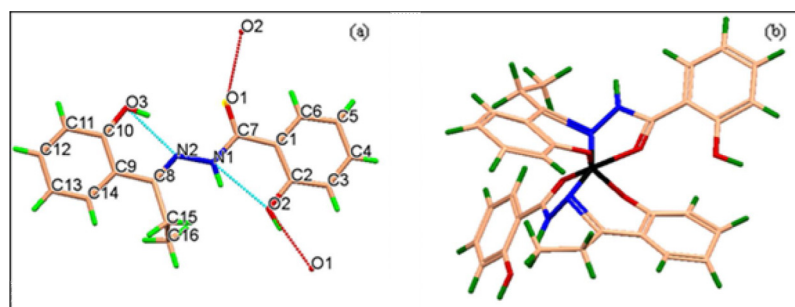


Fig. 8. a) Diagram showing inter and intramolecular H-bonding in hpsh (b) Proposed binding structure of hpsh- Cu^{2+} complex.

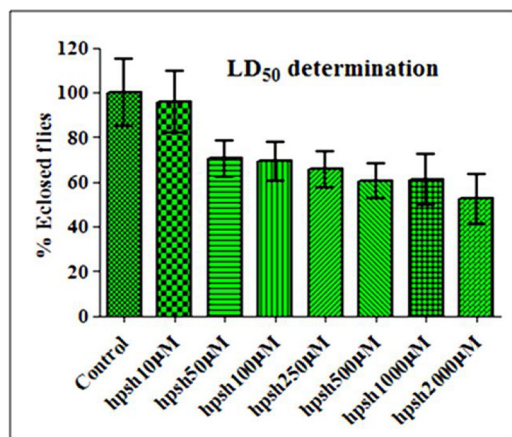


Fig. 9. The histogram represents percentage eclosed flies cultured in normal and hpsh treated food. The hpsh concentration 2000 µM is median lethal dose for *Drosophila* in which 50 % flies eclosion occurs.

bond formation or dipole-dipole interactions due to the presence of ICT [19].

3.8. LD₅₀ analysis and bioimaging

3.8.1. LD₅₀ analysis

To assess the 50 % lethal effects of hpsh on *Drosophila*, wild type flies were cultured in different concentrations of hpsh along with control in separate vials. Their F1 flies eclosion numbers were scored shown in graph (Fig. 9). The graph shows that flies grown in normal food represents total number of eclosed flies considered as control. Flies treated with 10 µM hpsh also exhibits normal eclosion number near to control. For evaluation of median lethal dose, result clearly shown in the following graph exhibited gradual decrease in eclosion number of flies with increase in hpsh concentrations. The administration of hpsh concentration 2000 µM exhibited nearly 50 % eclosion and 50 % death of fly population in contrast to control. Thus, present study confirmed that lower dose of hpsh is non-toxic and biocompatible for flies.

3.8.2. Bioimaging of adult fruit fly

In vivo studies of adult flies show that there is no fluorescence in blue channel and basal level of fluorescence (auto-fluorescence) in green channel in flies considered as control in (Fig. 10 A, B) while flies

treated with hpsh show strong fluorescence in abdominal region in green channel (Fig. 10C, D). Flies treated with Cu²⁺ alone exhibit results like control flies (Fig. 10E, F). It is clear from Fig. 10 that Cu²⁺ quenches the fluorescence of hpsh treated flies. (Fig. 10G, H) indicating the bioimaging property of hpsh in living system.

3.8.3. Bioimaging of gut tissue of fruit fly

The bioimaging of dissected gut tissue of fruit fly exhibits similar fluorescence properties like adult fruit fly (Fig. 11). Images (A–D) are the images of untreated gut tissue considered as control. It is clear from Fig. 11 (G) that tissue treated with hpsh exhibits strong green fluorescence while there is no fluorescence in tissue treated with Cu²⁺ alone (Fig. 11 K). The last panel of Fig. 11 represents complete fluorescence quenching of hpsh treated gut tissue after addition of Cu²⁺ in green channel (Fig. 11O).

4. Conclusions

In this study, we have reported a fluorescent probe, hpsh having large Stokes shift for selective and distinct quenching of Cu²⁺ ion in pure aqueous medium. The ground state complex formation of hpsh with Cu²⁺ reveals the quenching to be static in nature. The functioning of hpsh is regulated by intramolecular charge transfer (ICT) mechanism. Thus, hpsh could be applied as a highly selective fluorescence probe for Cu²⁺ ion without any interference. Moreover, according to the Jobs plot, a 1: 2 (M: L) stoichiometry between Cu²⁺ and hpsh is formed. The selectivity and cell-permeability of the probe state its plausible application in the biological signaling and tracking of copper.

CRedit authorship contribution statement

Romi Dwivedi: Conceptualization, Methodology, Visualization, Investigation, Data curation, Writing - original draft, Software. **Saumya Singh:** Resources. **Brijesh Singh Chauhan:** Investigation. **S. Srikrishna:** Formal analysis. **Anoop Kumar Panday:** Software. **Lokman H. Choudhury:** Software. **Vinod Prasad Singh:** Supervision, Validation.

Declaration of Competing Interest

There are no conflicts to declare.

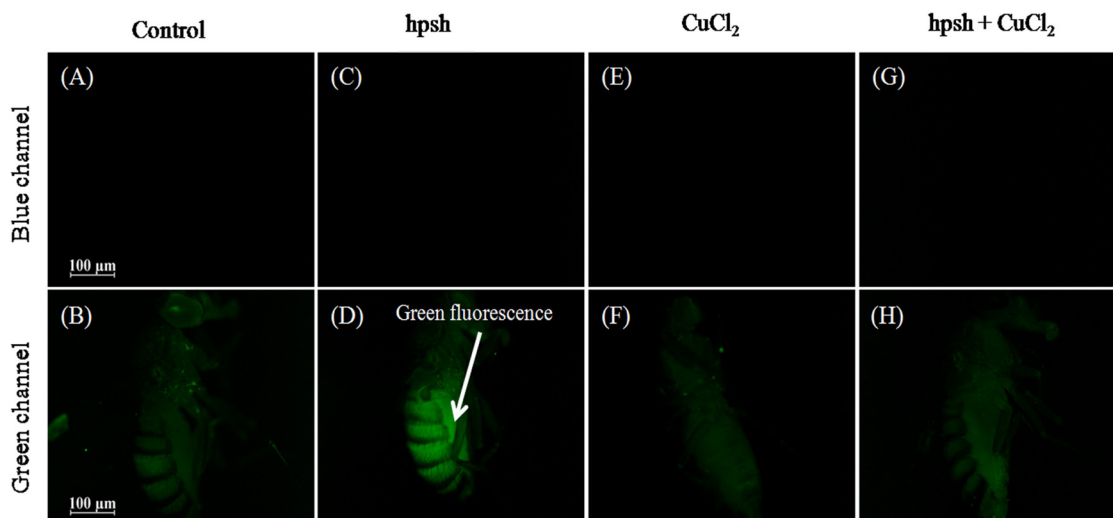


Fig. 10. *In vivo* images of adult fruit fly in blue and green channel fluorescence at 4X objective. Images (A) and (B) are considered as control flies, (C) and (D) are the hpsh treated flies showing fluorescence in green channel, (E) and (F) are the Cu²⁺ treated flies, (G) and (H) are the hpsh treated fly upon addition of Cu²⁺.

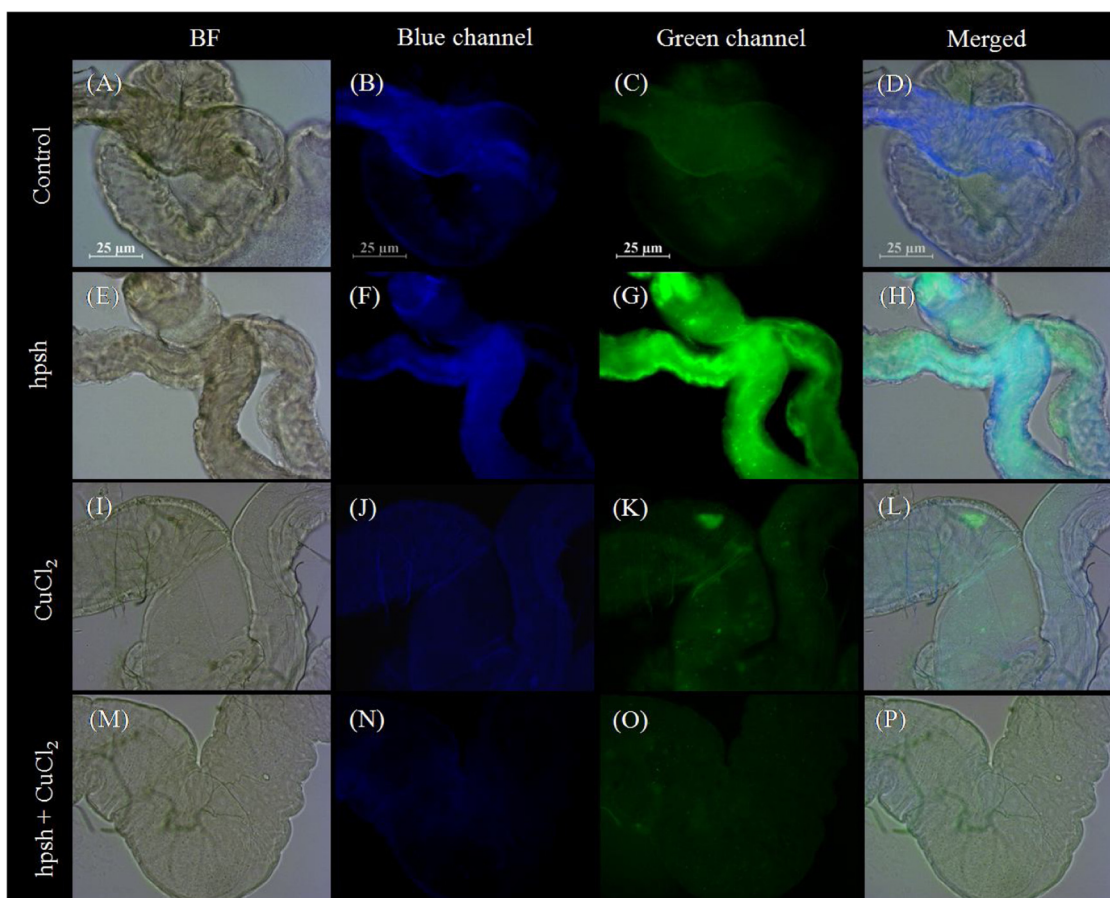


Fig. 11. *In vivo* images of adult fruit fly gut tissues at 20X objective. The control images (A-D) exhibit no fluorescence in blue and green channel. Images. Panel (E-H) represents fluorescence in green channel in hpsh (10 μM) treated tissue. Third panel (I-L) represents tissue incubated with Cu^{2+} only. Fourth panel (M-P) represents fluorescence quenching of hpsh treated tissue after addition of Cu^{2+} .

Acknowledgements

The authors thank the Head, S.A.I.F., Indian Institute of Technology, Patna, India for recording mass spectra and fluorescence data.

Appendix A. Supplementary data

Supplementary material related to this article can be found, in the online version, at doi:<https://doi.org/10.1016/j.jphotochem.2020.112501>.

References

- [1] D.T. Hogan, T.C. Sutherland, *New J. Chem.* 42 (2018) 16469–16473.
- [2] D.P. Singh, R. Dwivedi, A.K. Singh, B. Koch, P. Singh, V.P. Singh, *Sens. Actuators B* 238 (2017) 128–137.
- [3] S. Nagl, O.S. Wolfbeis, *Analyst* 132 (2007) 507–511.
- [4] A.J. Sanchez, B. Ortiz, V.O. Navarrete, N. Farfan, R. Santillan, *Analyst* 140 (2015) 6031–6039.
- [5] L. Yu, Y. Qu, F. Chai, L. Chen, *New J. Chem.* 42 (2018) 17478–17485.
- [6] E.D. Harris, *Nutr. Rev.* 59 (2001) 281–285.
- [7] J.L. Groff, S.S. Gropper, S.M. Hunt, *Advanced Nutrition and Human Metabolism*, West Publishing Company, New York, 1995.
- [8] S.G. Liu, N. Li, Y.Z. Fan, N.B. Li, H.Q. Luo, *Sens. Actuators B Chem.* 243 (2017) 634–641.
- [9] Y. Christen, *Am. J. Clin. Nutr.* 71 (2000) 621–629.
- [10] T. Saha, A. Sengupta, P. Hazra, P. Talukdar, *Photochem. Photobiol. Sci.* 13 (2014) 1427.
- [11] V. Dujols, F. Ford, A.W. Czarnik, *J. Am. Chem. Soc.* 119 (1997) 7386–7387.
- [12] L.P. Singh, J.M. Bhatnagar, *Talanta* 64 (2004) 313–319.
- [13] P.A. More, G.S. Shankarling, *Sens. Actuators B Chem.* 241 (2017) 552–559.
- [14] Z.C. Liu, Z.Y. Yang, T.R. Li, B.D. Wang, Y. Li, D.D. Qin, M.F. Wang, M.H. Yan, *Dalton Trans.* 40 (2011) 9370–9373.
- [15] W.L. Chang, P.Y. Yang, *J. Lumin.* 41 (2013) 38–43.
- [16] Y.W. Sie, C.F. Wan, A.T. Wu, *RSC Adv.* 7 (2017) 2460–2465.
- [17] P. Horváth, P. Sebej, T. Solomek, P. Kian, *J. Org. Chem.* 80 (2015) 1299–1311.
- [18] B. He, H. Nie, L. Chen, X. Lou, R. Hu, A. Qin, Z. Zhao, B.Z. Tang, *Org. Lett.* 17 (2015) 6174–6177.
- [19] S.O. Aderinto, Y. Xu, H. Peng, F. Wang, H. Wu, X. Fan, *J. Fluoresc.* 27 (2017) 79–87.
- [20] J. Bu, H. Duan, X. Wang, *Res. Chem. Intermed.* 40 (2014) 3119–3126.
- [21] M. Mishra, K. Tiwari, A.K. Singh, V.P. Singh, *Polyhedron* 77 (2014) 57–65.
- [22] H.A. Benesi, J.H. Hildebrand, *J. Am. Chem. Soc.* 71 (1949) 2703–2707.
- [23] B.P. Joshi, J. Park, W.I. Lee, K.H. Lee, *Talanta* 78 (2009) 903–909.
- [24] M.R. Eftink, *Fluorescence Quenching Reactions*, Plenum Press, New York, 1991, pp. 1–44.
- [25] J.R. Lakowicz, G. Weber, *Biochemistry* 12 (1973) 4161–4170.
- [26] D.P. Singh, B.K. Allam, K.N. Singh, V.P. Singh, *RSC Adv.* 4 (2014) 1155–1158.
- [27] P. Krishnamoorthy, P. Sathyadevi, A.H. Cowley, R.R. Butorac, N. Dharmaraj, *Eur. J. Med. Chem.* 46 (2011) 3376–3387.
- [28] R. Dwivedi, D.P. Singh, B.S. Chauhan, S. Srikrishna, A.K. Panday, L.H. Choudhury, V.P. Singh, *Sens. Actuators B Chem.* 258 (2018) 881–894.
- [29] P. Sathyadevi, P. Krishnamoorthy, R.R. Butorac, A.H. Cowley, N.S.P. Bhuvanesh, N. Dharmaraj, *Dalton Trans.* 40 (2011) 9690–9702.
- [30] V.L. Sii, M.R. Sudarsanakumar, S. Suma, *Polyhedron* 29 (2010) 2035–2040.
- [31] G.L. Long, J.D. Winefordner, *Anal. Chem.* 55 (1983) 712A–724A.
- [32] G.R. You, G.J. Park, J.J. Lee, C. Kim, *Dalton Trans.* 44 (2015) 9120–9129.
- [33] H.S. Jung, P.S. Kwon, J.W. Lee, J.I.I. Kim, C.S. Hong, J.W. Kim, S. Yan, J.Y. Lee, J.H. Lee, T. Joo, J.S. Kim, *J. Am. Chem. Soc.* 131 (2009) 2008–2012.
- [34] A.P. de Silva, B. McCaughan, B. McKinney, M. Querol, *Dalton Trans.* 10 (2003) 1902–1913.
- [35] J.F. Callan, A.P. de Silva, D.C. Magri, *Tetrahedron* 61 (2005) 8551–8588.
- [36] C. Yang, Y. Liu, D. Zheng, J. Zhu, J. Dai, *J. Photochem. Photobiol. A* 188 (2007) 51–55.
- [37] Y. Hu, Y. Liu, X. Xiao, *Biomacromolecules* 10 (2009) 517–521.
- [38] N.I. Georgiev, V.B. Bojinov, *J. Lumin.* 132 (2012) 2235–2241.